Ceramics-Silikáty 65 (4), 334-343 (2021)
www.ceramics-silikaty.cz doi: 10.13168/cs.2021.0035

SINTERING MECHANISM, STRUCTURE AND CRYSTALLISATION OF CaO-MgO-Al_2O_3-SiO_2 GLASS-CERAMICS FROM BLAST FURNACE SLAG

YUNFEI FAN*, #FENG HE*, **, ZIJIE LI*, ZUHAO LI*, WENTAO ZHANG*, JUNLIN XIE*

*School of Materials Science and Engineering, Wuhan University of Technology, Wuhan, 430070, China
**Wuhan University of Technology Chongqing Research Institute, Chongqing, 401122, China

#E-mail: he-feng2002@163.com

Submitted August 27, 2021; accepted September 14, 2021

Keywords: CMAS glass-ceramics, Sintering mechanism, Blast furnace slag, ZnO

CaO-MgO-Al_2O_3-SiO_2 glass-ceramics with different amounts of ZnO from blast furnace slag were prepared using the sintering method. The structure and properties of the glasses or glass-ceramics were investigated by Raman, DSC, HSM, XRD, and FE-SEM. The T_g and T_c of the glass decreased with an increase in the ZnO amount. As the ZnO content increased from 2 wt. % to 4 wt. %, the E_a of the glass decreased and the sinterability increased, while with any further increase in the ZnO content, the sinterability decreased. The Raman analysis showed that when the ZnO content was 4 wt. %, the adjustment of the glass structure was obvious. The relative area of Q^0 and Q^2 reached the maximum, and Q^1 and Q^3 reached the minimum, meanwhile, the main structure of the glass changed from Q^1 to Q^2. The main crystal phase of the glass-ceramics was akermanite; ZnO promoted the precipitation of akermanite, but inhibited the precipitation of diopside. With the increase in the ZnO content, the bulk density of the glass-ceramics increased while the flexural strength and microhardness decreased.

INTRODUCTION

CaO-MgO-Al_2O_3-SiO_2 (CMAS) glass-ceramics are widely used as architectural decoration materials and wear-resistant materials due to their high mechanical strength and wear resistance [1, 2]. Blast furnace slag (BFS) is an industrial waste, which is similar to CMAS glass-ceramics in composition. In recent years, the preparation of glass-ceramics has been considered as an effective way to recover BFS [3, 4, 5]. In the process of preparing glass-ceramics with BFS, some other oxides were added to adjust the preparation and properties of the glass-ceramics [6, 7, 8].

The melting method is a common method for the preparation of glass-ceramics from BFS [9, 10]. The content of CaO in the BFS is more than 35 wt. %, and the glass-ceramics prepared from BFS is a high calcium system. Zhang et al. [11] studied the crystallisation mechanism of glass-ceramics from BFS, and their results showed that an increase in CaO/SiO_2 led to a transition from bulk crystallisation to surface crystallisation, which resulted in insufficient crystallisation and was not conducive to improve the strength of glass-ceramics. The sintering method can make full use of the surface crystallisation of glass particles and prepare glass-ceramics with a high crystal phase content. However, the higher basicity of BFS leads to fast crystallisation, and the precipitation of a crystal phase on the surface of the glass particles hinders the sintering process, which is not conducive to the densification of glass-ceramics and the improvement of their properties [12]. Therefore, it is necessary to study the sinterability of glass.

The composition of glass-ceramics is related to the sinterability. The sintering process determines the crystallisation, structure and densification, which affect the properties of glass-ceramics. ZnO is a common additive in glass-ceramics, which has different effects on the sintering, structure, crystallisation and properties of glass-ceramics. Seidel [13] showed that the ZnO content was related to the crystal phase composition of glass-ceramics, and ZnO was also beneficial in improving the mechanical properties. ZnO can act as network modifier or network former, and Zn^{2+} can exist as [ZnO_4] and [ZnO_6] in glass structures [14, 15]. Chen [16] found that ZnO acted as a modifier in the glass network, increasing the density of glass, decreasing the glass transition temperature. Gui [17] reported that ZnO enhanced the glass-forming ability of glass when the addition of ZnO is low, and then weakened the glass-forming ability with a further increase in ZnO, furthermore, the thermal and

dielectric properties of glass-ceramics are also connected with ZnO. In the research on the preparation of glass-ceramics from BFS, the effect of ZnO on the structure and sintering of glass is seldom studied. ZnO acts as an addition to adjust the performance of BFS glass-ceramics, therefore, it is necessary to investigate the effect of ZnO on BFS glass-ceramics.

In this paper, CMAS glass-ceramics with different ZnO contents from BFS were prepared by the sintering method. The effects of ZnO on the sintering, crystallisation and properties of the glass-ceramics were studied. The Q^n units of the glass melt were investigated by Raman spectroscopy, while the connection between the structure and the sintering of the glass was revealed.

EXPERIMENTAL

Raw materials and experimental formula

The BFS used in this experiment was from China Baowu Iron & Steel Group. The chemical compositions of the BFS were measured by X-ray fluorescence (XRF, Zetium, PANalytical B. V.), and the results are shown in Table 1. This experiment was based on 60 wt. % BFS. SiO_2, Na_2O, K_2O, BaO, B_2O_3 and ZnO were introduced to modify the melting and sintering points of the samples. The oxides were introduced by Na_2CO_3, K_2CO3, $BaCO_3$, H_3BO_3 and ZnO, respectively. This experiment prepared the base glass with different ZnO additions, which were 2 wt. %, 3 wt. %, 4 wt. %, 5 wt. %, 6 wt. %, respectively, and their specific oxide compositions are shown in Table 1.

Preparation of the glass-ceramics

In this paper, the glass-ceramics were prepared by the sintering method. The base glass was melted at 1450 °C for 1 h. The melted glass liquid was poured into clear water to obtain the base glass slag. The glass slag was ground with a planetary grinding ball for 30 min and then passed through a 200-mesh sieve to obtain the parent glass powder. The parent glass powder was pressed into 4 mm × 40 mm strip samples under a pressure of 50 MPa for 2 min. Then the samples were sintered in a resistance furnace, the sintering temperature was determined by thermal analysis, the heating rate was 5 °C·min^{-1}.

Characterisations

The thermal behaviour of the glass powder was studied using Differential Scanning Calorimetry (DSC, STA449F3, NETZSCH) at 50 °C - 1000 °C and the heating rate was 5 °C·min^{-1}. The sintering shrinkage curve of the glass powder was measured by a Hot-Stage Microscope (HSM, HM867). The Raman spectra of the glass samples were measured using Raman spectrometer (LABHRev-UV) in the range of 400 cm^{-1} - 2000 cm^{-1}. The crystal phases of the glass-ceramics were measured by an X-ray diffractometer (XRD, D8 Advance, BRUKER AXS) at 10° - 70°. The morphology and element distribution of the glass-ceramics were observed by a Field Emission Scanning Electron Microscope (FE-SEM, Zeiss Ultra Plus, Zeiss Germany) with an Energy Dispersive Spectrometer (EDS; X-Max 50), the polished surface was etched with a HF solution (4 %) for 40 s. The bending strength (M, MPa) of the glass-ceramics was measured by the three-point test method. The bulk density of the glass-ceramics was measured by the Archimedes-drainage method. The indentation method was used to measure the Vickers hardness of the glass-ceramics, the loading force was 0.98 N, the loading time was 10 s.

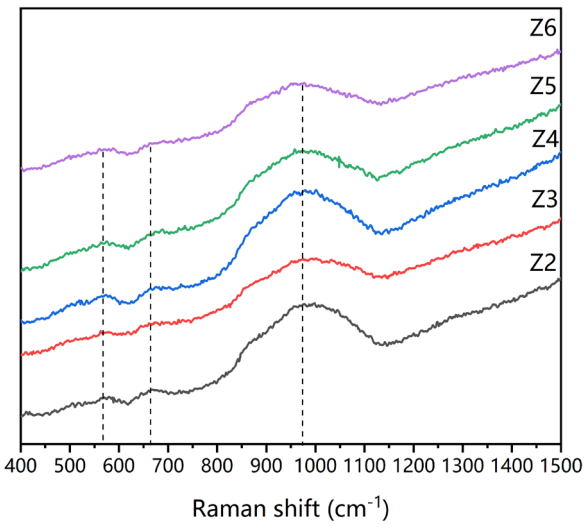

Figure 1. Raman spectra of base glasses with different ZnO.

Table 1. Oxide compositions of the glass and BFS (wt. %).

	Al_2O_3	SiO_2	CaO	MgO	BaO	Na_2O	K_2O	B_2O_3	ZnO	Other
BFS	15.12	31.92	39.81	8.54	0.12	0.39	0.58	/	/	3.52
Z2	9.07	46.19	23.89	5.12	3.00	3.00	3.00	2.00	2.00	2.73
Z3	9.07	45.19	23.89	5.12	3.00	3.00	3.00	2.00	3.00	2.73
Z4	9.07	44.19	23.89	5.12	3.00	3.00	3.00	2.00	4.00	2.73
Z5	9.07	43.19	23.89	5.12	3.00	3.00	3.00	2.00	5.00	2.73
Z6	9.07	42.19	23.89	5.12	3.00	3.00	3.00	2.00	6.00	2.73

RESULTS AND DISCUSSION

Raman spectra analysis

Figure 1 showed the Raman spectra of the glass. There were three Raman peaks in all the glass samples; the peak located at 800 cm^{-1} - 1150 cm^{-1} had the largest FWHM, which was assigned to the stretching vibration of Si-O in [SiO_4] [18, 19, 20]. The Raman peak located at 800 cm^{-1} - 1150cm^{-1} was deconvoluted into different Q^n (n is the number of bridging oxygen atoms in [SiO_4]) [21, 22], the results were showed in Figure 2, and the Raman shift and relative area of Q^n are shown in Figure 3. The Raman shift of Q^n can be seen as consistent in Figure 3a), with the increase of ZnO, the Raman shift of Q^n first decreased, reaching the minimum at Z4, and then increased. Montoya-Quesada [23] showed that in a CaO-SiO_2-Al_2O_3 system, ZnO can act as a network modifier and network former with a change in the ZnO content. We assumed that when the ZnO content was less than 4 wt. %, ZnO mainly acted as network modifier, and weakened the Si-O, while with the ZnO addition of more than 4 wt. %, ZnO acted as a network former and polymerised the glass structure.

Figure 3b shows that, in the Z4 sample, an inflection point appeared in the relative area of Q^n, indicating that the adjustment of the glass structure was obvious here. The relative area of Q^0 and Q^2 reached the maximum, and Q^1 and Q^3 reached the minimum in the Z4 sample, meanwhile, the main structure of the glass changed from Q^1 to Q^2 in the Z4 sample. Zhang [24] also showed that there was a certain conversion relation between Q^1 and Q^2.

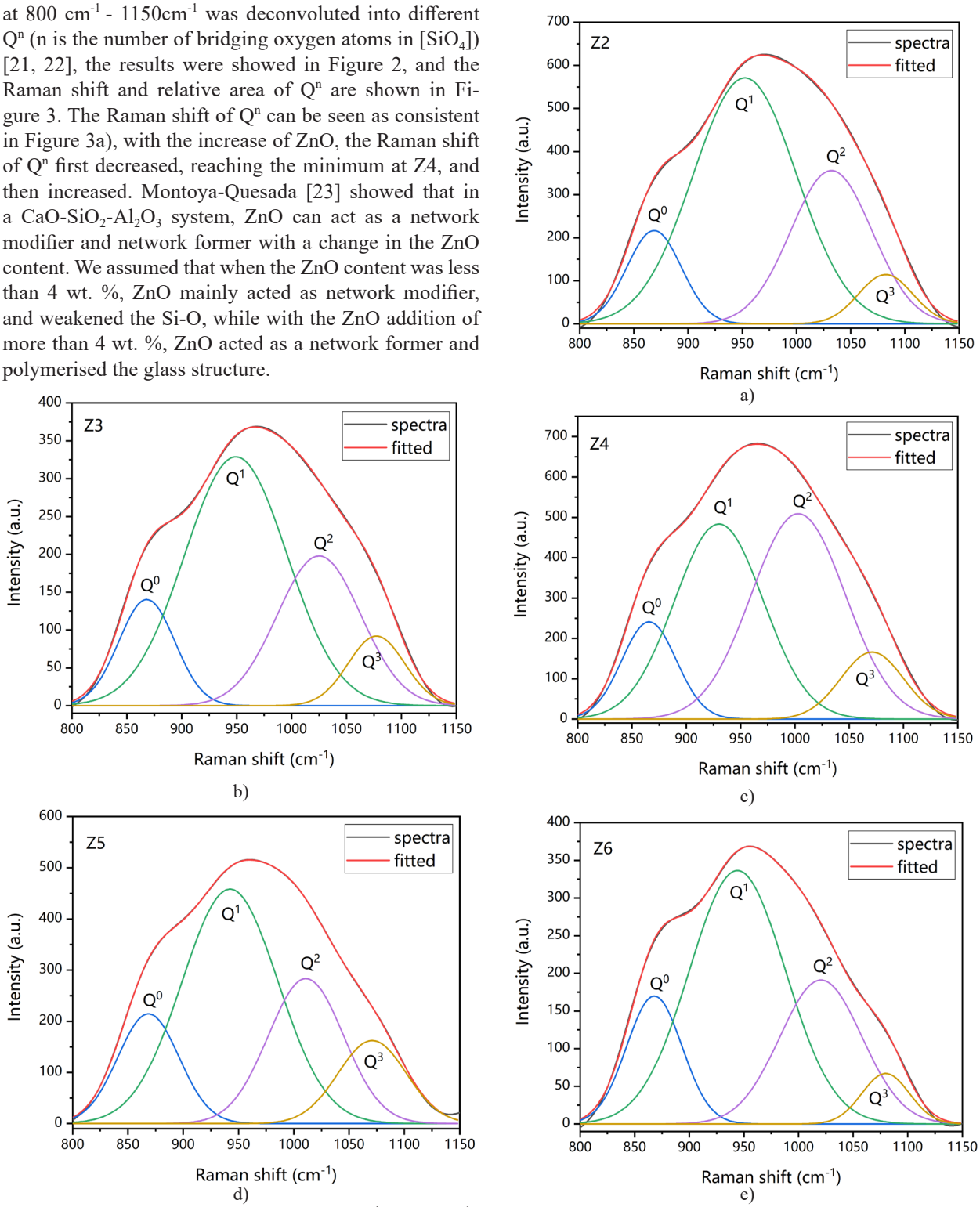

Figure 2. Deconvoluted Raman spectra (800 cm^{-1} - 1150 cm^{-1}) of the glasses using Gaussian type function.

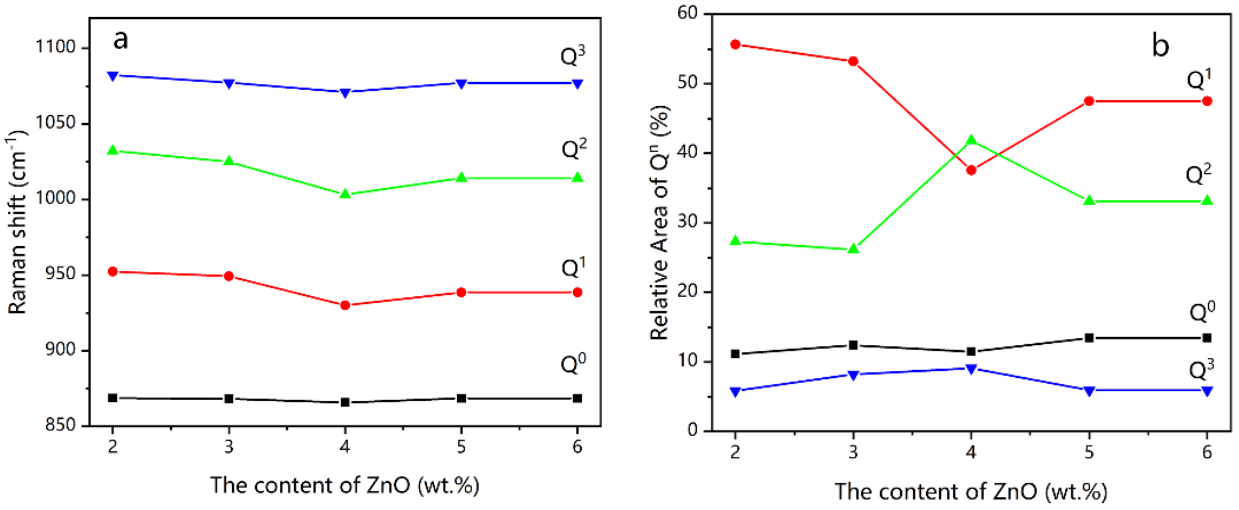

a) b)

Figure 3. Raman shift (a) and relative area (b) of Q^n in the glass samples.

Thermal analysis

The thermal properties of the glass are shown in Figure 4, there was an obvious exothermic peak in the range of 880 °C to 930 °C as shown in Figure 4a, indicating that the crystallisation occurred in this temperature range, while the glass transition temperature (T_g) is located around 650 °C. In Figure 4b, the volume of the sample shrunk sharply which is located around 800 °C, where there was an obvious endothermic valley in the DSC, which indicated that sintering occurred rapidly around 800 °C. According to the results of the thermal analysis (5 °C·min^{-1}) of the glass powder, all the glass samples were sintered at 930 °C for 1.5 h.

The sintering profile of the glass is shown in Figure 5, and the characteristic temperatures are listed in Table 2, in which T_{fs} is the first sintering temperature, T_{ms} is the maximum sintering temperature, T_{me} is the maximum expansion temperature (when the height of the sample reached the maximum), T_h is the hemisphere temperature, T_m is the melting temperature, T_c is the crystallisation temperature, $S_c = T_c - T_{ms}$, is the sintering parameter, the larger the S_c is, the more independent the crystallisation and sintering process is [25]. With an increase in the ZnO content, the T_g and T_c decreased gradually, the T_{fs} and T_{ms} of the samples decreased first and then increased, while the S_c value increased first and then decreased. Meanwhile, in the Z4 sample, T_{fs} and T_{ms}

Table 2. Characteristic temperature of the glass with different ZnO contents.

	T_g	T_{fs}	T_{ms}	T_c	T_{me}	T_h	T_m	S_c
Z2	662.1	754.7	861.7	928.1	1166.3	1180.0	1209.0	66.4
Z3	651.1	746.2	846.0	923.1	1170.8	1193.0	1217.0	77.1
Z4	643.6	740.9	833.1	921.8	1162.4	1196.0	1219.0	88.7
Z5	639.0	741.0	834.3	918.3	1170.5	1199.1	1212.0	84.0
Z6	633.7	741.3	820.7	883.7	1183.2	1218.1	1238.1	63.0

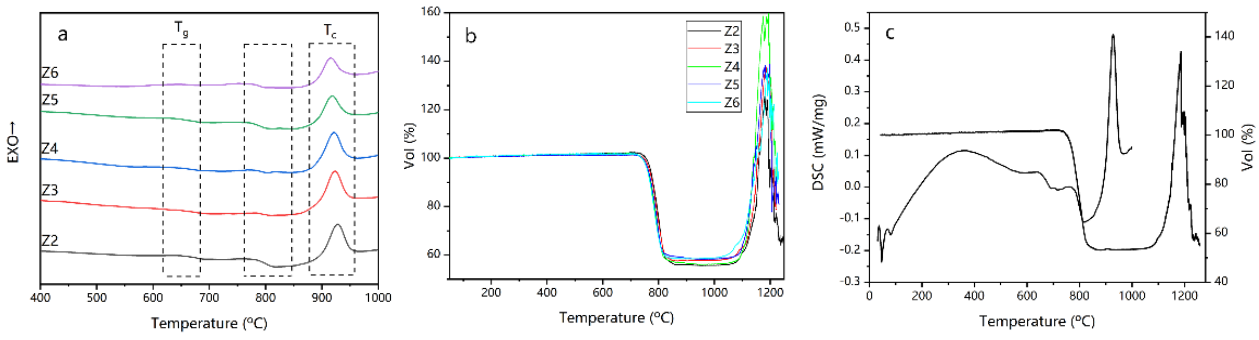

a) b) c)

Figure 4. Thermal properties of the glass with different ZnO contents at 5 °C/min (a: DSC curve, b: sintering shrinkage curve, c: comparison between the DSC curve and sintering shrinkage curve of Z2).

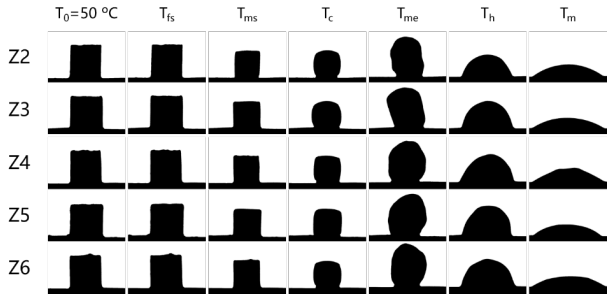

Figure 5. Sintering shrinkage diagrams of the glass with different ZnO contents at 5 °C·min^{-1}.

reached the minimum, while S_c reached the maximum. This indicated that the sinterability of the glass samples changed with an increase in the ZnO content. Dechandt [25] showed that in a SiO_2-Al_2O_3-MgO system, ZnO improved the sinterability by decreasing the T_{fs} and T_{ms} and increasing the S_c.

In order to further explore the sintering behaviour, the sintering shrinkage curves were measured to calculate the sintering activation energy at different heating rates. Figure 6 shows the sintering shrinkage curves of the glass powders with the different ZnO contents at 5 °C·min^{-1}, 10 °C·min^{-1}, 15 °C·min^{-1}, and 25 °C·min^{-1}. The sintering activation energy was calculated by the Arrhenius formula [26, 27]:

$$\ln k = \frac{-E_a}{R}\left(\frac{1}{T}\right) + A \quad (1)$$

Where, k is the heating rate, E_a is the sintering activation energy, T is the absolute temperature, R is the gas constant (8.3145 J·(K·mol^{-1})$^{-1}$), and A is a constant.

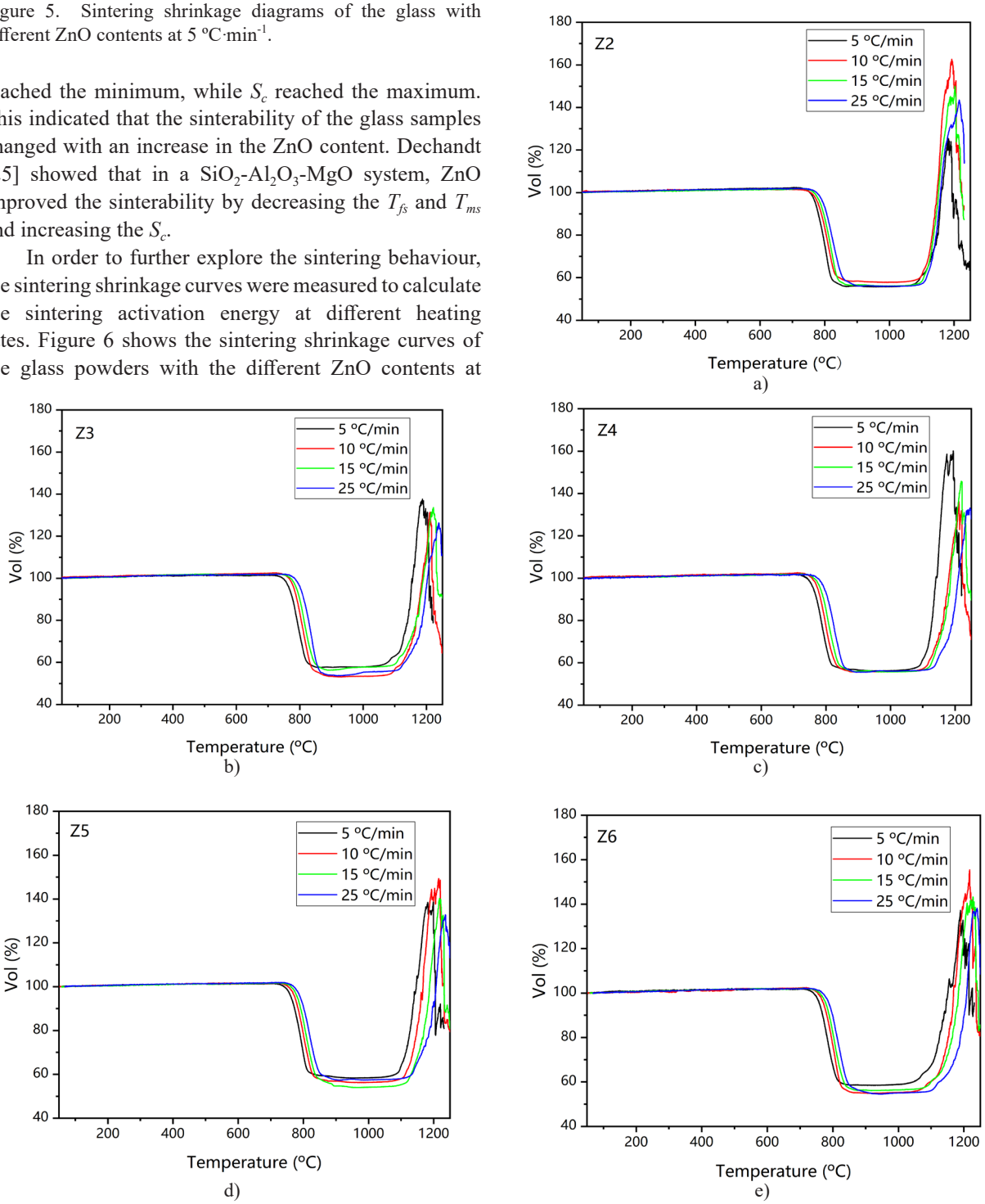

Figure 6. Sintering shrinkage curves of the glass with different ZnO contents at 5 °C·min^{-1}, 10 °C·min^{-1}, 15 °C·min^{-1}, 25 °C·min^{-1}.

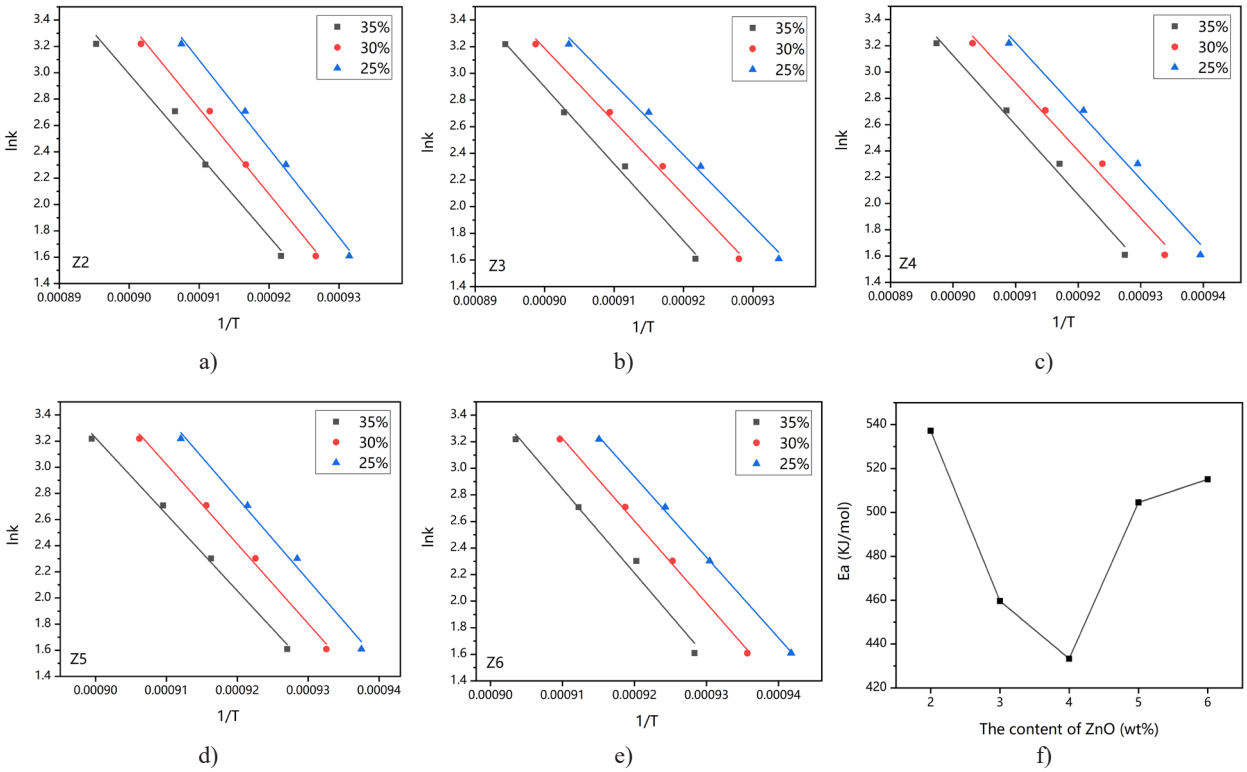

Figure 7. Fitting curves and sintering activation energy of the glass with the different ZnO contents.

The fitting curves of ln k and $1/T$ were performed when the volume shrinkage was 25 %, 30 % and 35 %, respectively. E_a was calculated from the slope of ln k and $1/T$, and the average values of the three curves were taken as the final E_a results, which are shown in Figure 7, the average E_a were 537.2 kJ·mol^{-1}, 459.6 kJ·mol^{-1}, 433.4 kJ·mol^{-1}, 504.5 kJ·mol^{-1}, 515.1 kJ·mol^{-1}, respectively. With an increase in the ZnO, the E_a first decreased, reaching the minimum at Z4, and then increased, which was consistent with the change in the T_{fs} and T_{ms}. It showed that the sinterability of the glass powder was the best when the content of ZnO was 4 wt. %.

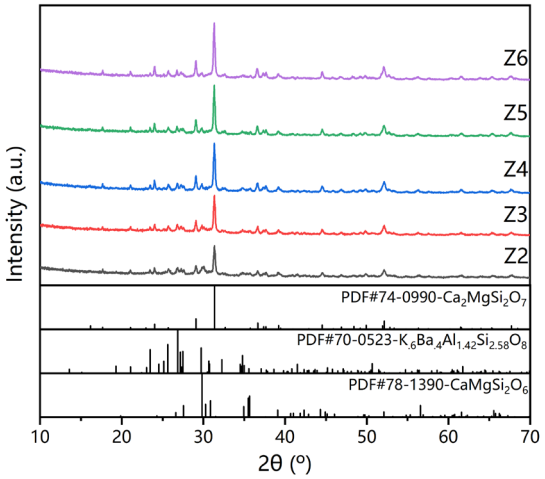

Figure 8. XRD patterns of the glass-ceramics with the different ZnO contents.

The results of the Raman analysis showed that the structure of the glass in Z4 was significantly different, ZnO acted mainly as a network modifier, destroying the network, which reduced the liquid viscosity and promoted ion diffusion. However, in the Z5 and Z6 samples, ZnO acted mainly as a network former, and connected the network. Meanwhile, the decrease in the SiO_2 in glass was not conducive to the generation of liquid in the sintering process. The results of the Raman analysis and thermal analysis showed that the decrease of Q^0 and Q^1 units and the increase of Q^2 and Q^3 units were beneficial to improve the sinterability of the glass powder.

Crystal phase analysis

The XRD patterns of the glass-ceramics with the different ZnO contents are illustrated in Figure 8. Akermanite ($Ca_2MgSi_2O_7$, PDF#74-0990) was identified as the main crystal phase, diopside ($CaMgSi_2O_6$, PDF#78-1390) and hyalophane ($K_{.6}Ba_{.4}Al_{1.42}Si_{2.58}O_8$, PDF#70-0523) accompanied the crystal phases. With an increase in the ZnO content, the diffraction peak intensity of akermanite increased gradually, while the diffraction peak intensity of diopside decreased, illustrating that ZnO was beneficial to the precipitation of akermanite, and hindered the precipitation of diopside.

Figure 9 shows the FE-SEM morphology of the glass-ceramics. In the Z2 and Z3 samples, block and rodlike grains grew separately, while in the Z4 and Z5

samples, grains grew and connected together. The EDS mapping (Figure 10) of the Z2 glass-ceramics revealed different morphologies, one of which was crystals richer in Mg and poorer in K, suggesting it was akermanite or diopside. The atomic percentage distribution (%) of the elements in Table 3 show that K and Ba in point 2 and point 3 were obviously higher than those in point 1, suggesting the rodlike crystal was hyalophane. Since the content of ZnO was low and did not participate in the crystal phase, the Zn was evenly distributed in the sample in Figure 10.

Physical and mechanical properties analysis

Figure 11 shows the properties of the glass-ceramics with the different ZnO contents. The bulk density of the glass-ceramics was between 2.738 g·cm^{-3} to 2.839 g·cm^{-3}, the bending strength was between 112.6 MPa to 156.1 MPa and the microhardness was between 476.6 Hv to 564.2 Hv. In Figure 11a, the bulk density increased gradually with an increase in the ZnO content, because the ZnO density was higher than that of most of the raw materials [23].

On the contrary, Figure 11b and Figure 11c show that the bending strength and microhardness of the glass-ceramics decreased with an increase in the ZnO content. Diopside is a kind of crystal phase with excellent mechanical properties [28, 29]. The increase in the ZnO content inhibited the precipitation of diopside. Meanwhile, ZnO promoted the precipitation and growth of akermanite, and the internal stress was easily generated between the growing grains, which reduced the mechanical properties of the glass-ceramics.

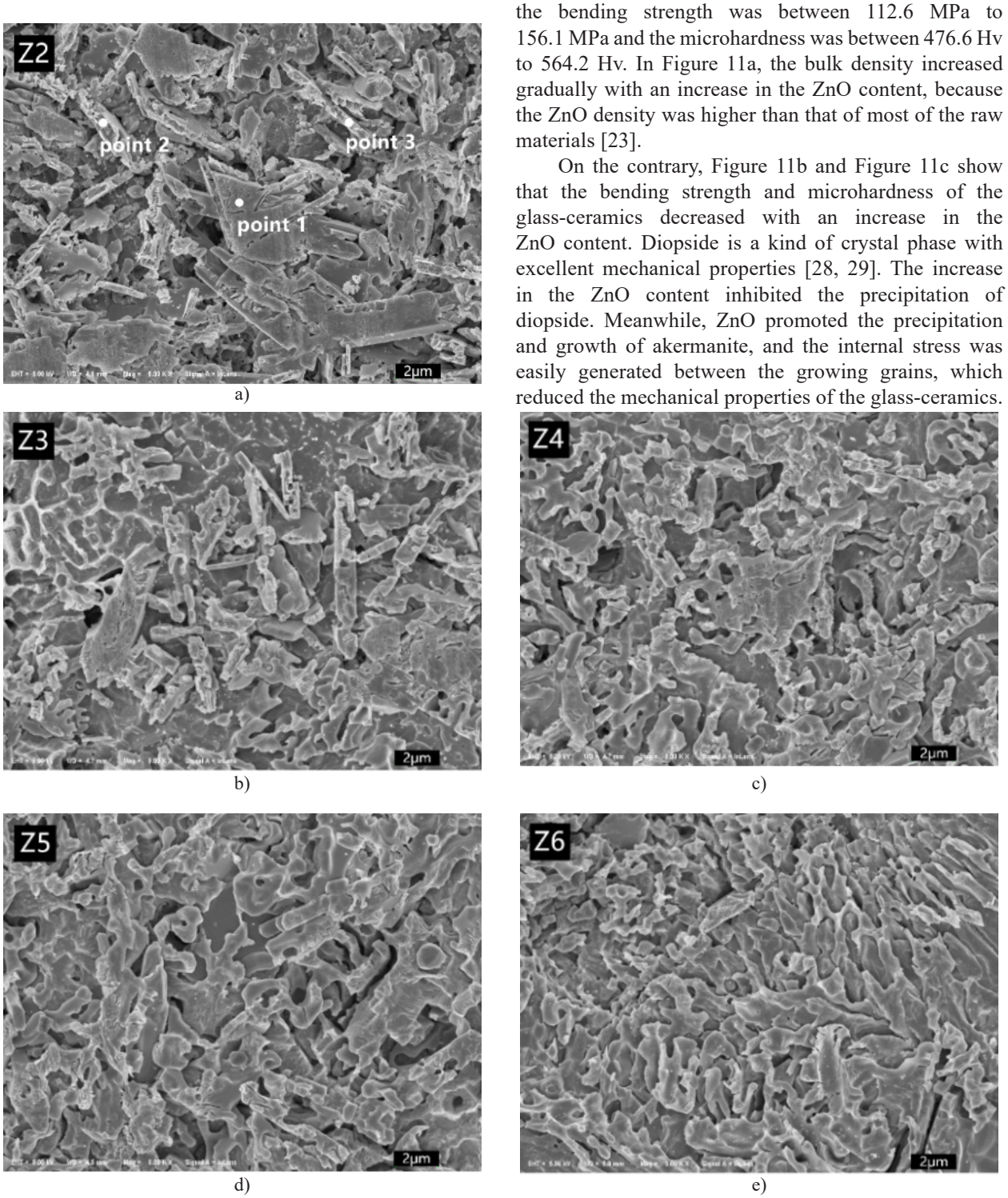

Figure 9. FE-SEM morphology of the glass-ceramics with the different ZnO contents.

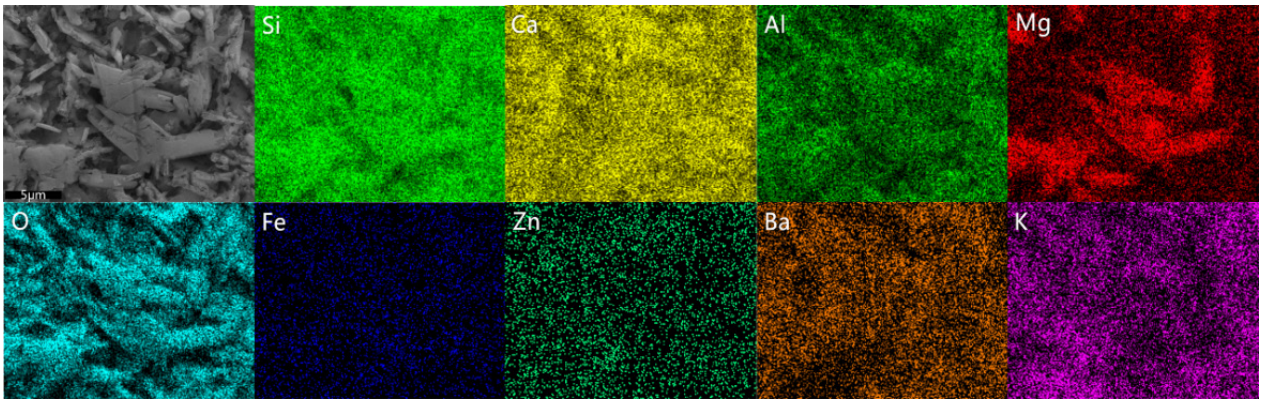

Figure 10. EDS mapping of the glass-ceramics with 2 wt. % ZnO (Z2).

Table 3. The atomic percentage distribution (%) of the elements in the glass-ceramics with 2 wt. % ZnO (Z2) at different points.

	O	Na	Mg	Al	Si	K	Ca	Ti	Fe	Zn	Ba	Total
Point 1	70.17	1.19	3.70	4.04	13.56	0.62	5.46	0.37	0.18	0.25	0.46	100
Point 2	68.96	1.36	1.17	5.59	14.53	1.38	5.30	0.24	0.16	0.30	1.01	100
Point 3	68.46	1.24	1.48	4.86	15.01	1.17	6.37	0.25	0.12	0.26	0.78	100

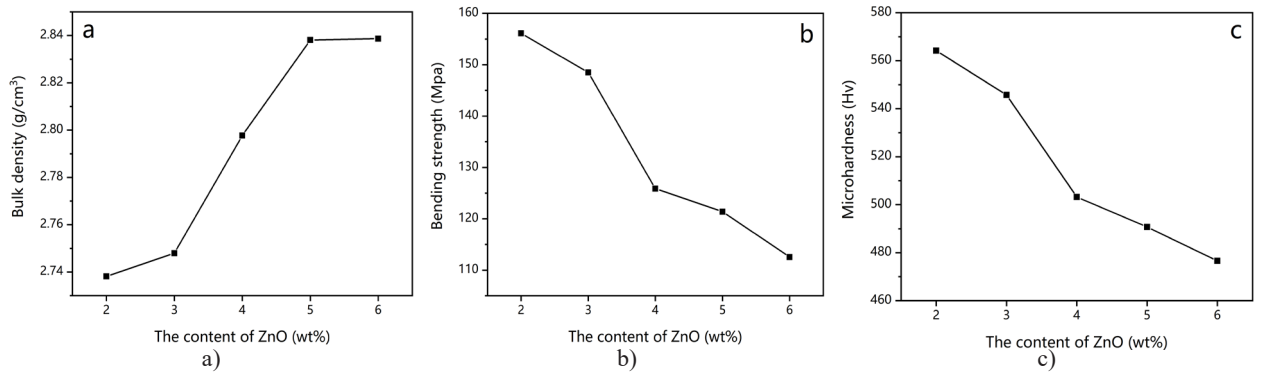

Figure 11. Properties of the glass-ceramics with the different ZnO contents. a) bulk density; b) bending strength; c) microhardness

In the results of Figure 11a, Figure 11b and Figure 11c, the increase (decrease) in the ratio of the volume density, bending strength and microhardness of Z4 glass ceramics were significant, which was related to the high sinterability of the Z4 glass powder.

CONCLUSION

In this paper, CMAS glass-ceramics with different ZnO contents were prepared by the sintering method from BFS. The connection between the structure and the sinterability of the glass powder was studied and some interesting phenomena were found. As the ZnO content increased from 2 wt. % to 4 wt. %, the E_a of the glass decreased, and the sinterability increased, while with a further increase in the ZnO content, the sinterability decreased. The Raman analysis showed that this variation was related to the Q^n. With an increase in the ZnO content, the Raman peak of Q^n first moved to low frequencies, reaching the lowest frequency in the Z4 sample, and then moved to high frequencies. The Q^1 unit dominated the glass network, while with an increase in the ZnO content, the Q^1 unit decreased. When the ZnO content was 4 wt. %, Q^1 decreased sharply, while Q^2 increased and dominated the glass network. With a further increase in the ZnO content, Q^2 decreased and Q^1 increased, and Q^1 dominated the glass network. The T_g and T_c of the glass decreased with an increase in the ZnO content. The main crystal phase of the glass-ceramics was akermanite, ZnO promoted the precipitation of akermanite, but inhibited the precipitation of diopside. With an increase in the ZnO content, the bulk density of the glass-ceramics increased, while the flexural strength and microhardness decreased. In the Z4 simple, the best sinterability caused the bulk density to change the most significantly. When the ZnO content was 2 wt. %, the mechanical properties of the glass-ceramics were the best, with a bulk density of 2.848 g·cm^{-3}, a bending strength of 156.1 MPa and a microhardness of 564.2 Hv.

Acknowledgment

We acknowledge Dr. Yumei Li (Center for Material Research and Analysis, Wuhan University of Technology,

China) for the FE-SEM analyses. This work was supported by the research project of Wuhan University of Technology Chongqing Research Institute (JZ2021-03).

REFERENCES

1. [1] Akatsuka K., Yasumori A., Maeda K. (2019): Structure of crystalline CaAl2Si2O8 precipitated in a CaO--Al_2O_3-SiO_2 glass-ceramic. Materials Letters, 242, 163-165. doi: 10.1016/j.matlet.2018.12.080
[2] Deng L., Zhang X., Zhang M., Jia X. (2018): Effect of CaF_2 on viscosity, structure and properties of CaO-Al_2O_3-MgO-SiO_2 slag glass ceramics. Journal of Non-Crystalline Solids, 500, 310-316. doi: 10.1016/j.jnoncrysol.2018.08.018
[3] Chen J., Yan B., Li H., Li P., Guo H. (2018): Vitrification of blast furnace slag and fluorite tailings for giving diopside-fluorapatite glass-ceramics. Materials Letters, 218, 309-312. doi: 10.1016/j.matlet.2018.02.020
[4] Zhang W., He F., Xiao Y., Xie M., Xie J., Sun R., Yang H., Luo Z. (2019): Effects of Al/Na and heat treatment on the structure and properties of glass ceramics from molten blast furnace slag. Ceramics International, 45(11), 13692-13700. doi: 10.1016/j.ceramint.2019.04.064
[5] Gao H. T., Liu X. H., Chen J. Q., Qi J. L., Wang Y. B. (2018): Preparation of glass-ceramics with low density and high strength using blast furnace slag, glass fiber and water glass. Ceramics International, 44(6), 6044-6053. doi: 10.1016/j.ceramint.2017.12.228
[6] Chen K., Li Y., Meng X., Meng L., Guo Z. (2019): New integrated method to recover the TiO_2 component and prepare glass-ceramics from molten titanium-bearing blast furnace slag. Ceramics International, 45(18), 24236-24243. doi: 10.1016/j.ceramint.2019.08.134
[7] Ding L., Ning W., Wang Q., Shi D., Luo L. (2015): Preparation and characterization of glass-ceramic foams from blast furnace slag and waste glass. Materials Letters, 141, 327-329. doi: 10.1016/j.matlet.2014.11.122
[8] Du Y., Ma J., Shi Y., Zhang X., Zhang H., Chen H., Ouyang S., Li B. (2020): Crystallization characteristics and corrosion properties of slag glass-ceramic prepared from blast furnace slag containing rare earth. Journal of Non-Crystalline Solids, 532, 119880. doi: 10.1016/j.jnoncrysol.2019.119880
[9] Deng L., Zhang X., Zhang M., Jia X., Zhang Z., Li B. (2019): Structure and properties of in situ synthesized $FeSi_2$-diopside glass ceramic composites from Bayan Obo tailings, blast furnace slag, and fly ash. Journal of Alloys and Compounds, 785, 932-943. doi: 10.1016/j.jallcom.2019.01.260
[10] Deng L., Jia R., Yun F., Zhang X., Li H., Zhang M., Jia X., Ren D., Li B. (2020): Influence of Cr_2O_3 on the viscosity and crystallization behavior of glass ceramics based on blast furnace slag. Materials Chemistry and Physics, 240, 122212. doi: 10.1016/j.matchemphys.2019.122212
[11] Zhang W., He F., Xie J., Liu X., Fang D., Yang H., Luo Z. (2018): Crystallization mechanism and properties of glass ceramics from modified molten blast furnace slag. Journal of Non-Crystalline Solids, 502, 164-171. doi: 10.1016/j.jnoncrysol.2018.08.024
[12] Chen L., Ge X., Long Y., Zhou M., Wang H., Chen X. (2020): Crystallization and properties of high calcium glass-ceramics synthesized from ferromanganese slag. Journal of Non-Crystalline Solids, 532, 119864. doi: 10.1016/j.jnoncrysol.2019.119864
[13] Seidel S., Dittmer M., Höland W., Rüssel C. (2017): High-strength, translucent glass-ceramics in the system MgO-ZnO-Al_2O_3-SiO_2-ZrO_2. Journal of the European Ceramic Society, 37(7), 2685-2694. doi: 10.1016/j.jeurceramsoc.2017.02.039
[14] Hao X., Luo Z., Hu X., Song J., Tang Y., Lu A. (2016): Effect of replacement of B_2O_3 by ZnO on preparation and properties of transparent cordierite-based glass-ceramics. Journal of Non-Crystalline Solids, 432, 265-270. doi: 10.1016/j.jnoncrysol.2015.10.017
[15] Chen G.H., Liu X.Y. (2007): Sintering, crystallization and properties of MgO-Al_2O_3-SiO_2 system glass-ceramics containing ZnO. Journal of Alloys and Compounds, 431 (1-2), 282-286. doi: 10.1016/j.jallcom.2006.05.060
[16] Chen L., Dai Y. (2016): Structure, physical properties, crystallization and sintering of iron-calcium-aluminosilicate glasses with different amounts of ZnO. Journal of Non-Crystalline Solids, 452, 45-49. doi: 10.1016/j.jnoncrysol.2016.08.017
[17] Gui H., Li C., Lin C., Zhang Q., Luo Z., Han L., Liu J., Liu T., Lu A. (2019): Glass forming, crystallization, and physical properties of MgO-Al_2O_3-SiO_2-B_2O_3 glass-ceramics modified by ZnO replacing MgO. Journal of the European Ceramic Society, 39(4), 1397-1410. doi: 10.1016/j.jeurceramsoc.2018.10.002
[18] Stavrou E., Palles D., Kamitsos E. I., Lipovskii A., Tagantsev D., Svirko Y., Honkanen S. (2014): Vibrational study of thermally ion-exchanged sodium aluminoborosilicate glasses. Journal of Non-Crystalline Solids, 401, 232-236. doi: 10.1016/j.jnoncrysol.2013.12.017
[19] Feng C., Gao L., Tang J., Liu Z., Chu M. (2020): Effects of MgO/Al_2O_3 ratio on viscous behaviors and structures of MgO-Al_2O_3-TiO_2-CaO-SiO_2 slag systems with high TiO_2 content and low CaO/SiO_2 ratio. Transactions of Nonferrous Metals Society of China, 30(3), 800-811. doi: 10.1016/S1003-6326(20)65255-4
[20] Shi Y., Han X., Li B., Chen Y., Zhang M. (2020): Modification of glass network and crystallization of CaO-Al_2O_3-MgO-SiO_2 based glass ceramics with addition of iron oxide. Ceramics International, 46(7), 9207-9217. doi: 10.1016/j.ceramint.2019.12.173
[21] Jia R., Deng L., Yun F., Li H., Zhang X., Jia X. (2019): Effects of SiO_2/CaO ratio on viscosity, structure, and mechanical properties of blast furnace slag glass ceramics. Materials Chemistry and Physics, 233, 155-162. doi: 10.1016/j.matchemphys.2019.05.065
[22] Zheng W., Cui J., Sheng L., Chao H., Peng Z., Shen C. (2016): Effect of complex nucleation agents on preparation and crystallization of CaO-MgO-Al_2O_3-SiO_2 glass-ceramics for float process. Journal of Non-Crystalline Solids, 450, 6-11. doi: 10.1016/j.jnoncrysol.2016.07.026
[23] Montoya-Quesada E., Villaquiran-Caiced M.A., de Gutierrez R.M., Munoz-Saldana J. (2020): Effect of ZnO content on the physical, mechanical and chemical properties of glass-ceramics in the CaO-SiO_2-Al_2O_3 system. Ceramics International, 46(4), 4322-4328. doi: 10.1016/j.ceramint.2019.10.154
[24] Zhang W., He F., Xiao Y., Xie M., Xie J., Li F., Yang H.,

Li Z. (2020): Structure, crystallization mechanism, and properties of glass ceramics from molten blast furnace slag with different B_2O_3/Al_2O_3. Materials Chemistry and Physics, 243, 122664. doi: 10.1016/j.matchemphys.2020.122664

[25] Dechandt I. C. J., Soares P., Pascual M. J., Serbena F. C. (2020): Sinterability and mechanical properties of glass-ceramics in the system SiO_2-Al_2O_3-MgO/ZnO. Journal of the European Ceramic Society, 40(15), 6002-6013. doi: 10.1016/j.jeurceramsoc.2020.07.032

[26] Zhou C., Yang J., Lin H., Zhang F., Ren L. (2019): Sintering Behavior and Microwave Dielectric Properties of BBSZL Glass-doped $ZnTiO_3$ Ceramics for LTCC Applications. Journal of Wuhan University of Technology-Materials Science Edition, 34(2), 282-286. doi: 10.1007/s11595-019-2047-5

[27] Parvatheeswara Rao B., Subba Rao P. S. V., Rao K. H. (1997): Densification, Grain Growth and Microstructure of Ni-Zn Ferrites. Journal de Physique IV (Proceedings), 7(C1), C1-241-C1-42. doi: 10.1051/jp4:1997192

[28] Kim E. S., Yeo W. J. (2012): Thermal properties of CaMgSi2O6 glass-ceramics with Al_2O_3. Ceramics International, 38, S547-S550. doi: 10.1016/j.ceramint.2011.05.074

[29] Shi Y., Han X., Li B., Chen Y., Zhang M. (2020): Modification of glass network and crystallization of CaO-Al_2O_3-MgO-SiO_2 based glass ceramics with addition of iron oxide. Ceramics International, 46(7), 9207-9217. doi: 10.1016/j.ceramint.2019.12.173